Macroscopic and microscopic description of low-energy collective states in ^{86,88}Se

G. Thiamova and Y. Grachev
Université Grenoble Alpes 1, CNRS, LPSC, Institut Polytechnique de Grenoble, N2P3, F-38026 Grenoble, France

M. Abolghasem
Department of Physics, VŠB - Technical University Ostrava, 17 Listopadu 15, CZ-708 33 Ostrava, Czech Republic

P. Alexa
Department of Physics and Institute of Clean Technologies, VŠB - Technical University Ostrava, 17 Listopadu 15, CZ-708 33 Ostrava, Czech Republic

P.-G. Reinhard
Institute for Theoretical Physics II, University of Erlangen, Staudstraße 7, D-91058 Erlangen, Germany

T. R. Rodríguez
Departamento de Física Teórica and Centro de Investigación Avanzada en Física Fundamental-CIAFF, Universidad Autónoma de Madrid, E-28049 Madrid, Spain

G. S. Simpson
Université Grenoble Alpes 1, CNRS, LPSC, Institut Polytechnique de Grenoble, IN2P3, F-38026 Grenoble, France

(Received 27 July 2018; revised manuscript received 5 October 2018; published 4 December 2018)

Algebraic collective model (ACM) calculations for the even-even selenium isotopes ^{86,88}Se have been performed to describe collective properties of these two transitional nuclei with only two and four valence neutrons, respectively. From the perspective of the ACM the nuclei turn out to be only weakly deformed, described by a very γ-soft potential. This is confirmed by Skyrme and Gogny energy density functional calculations. Additionally, the fully microscopic symmetry conserving configuration mixing method with the Gogny interaction has been applied to the study of these isotopes. The results show the transitional character of ^{86}Se and the relevant role of the triaxial degree of freedom in the structure of these nuclei.

DOI: 10.1103/PhysRevC.98.064304

I. INTRODUCTION

The study of neutron-rich nuclei in the mass region $A \approx 100$ region constitutes one of the main topics of modern nuclear structure physics and astrophysics. The investigation of their structure is an important source of information about their properties and production, and at the same time enables different theoretical models to be tested in extreme conditions.

Basic aspects of the transition between spherical and deformed shapes may be obtained using a simple model like the algebraic collective model (ACM) [1] employed in this paper. A shape transition occurs over a series of adjacent nuclei whose degree of deformation can usually be well estimated on the basis of the number of protons and neutrons in the valence shells. However, more microscopically based arguments, like the particular nuclear orbits involved, may also influence the onset of deformation.

From a structural point of view, a spherical nucleus is one for which single-particle modes dominate while a deformed nucleus contains a strong collective component in its wave function. One way to picture a transitional nucleus is one in which both $\beta = 0$ and $\beta \neq 0$ are energetically accessible without a significant energetic preference for the spherical or the deformed minimum. The range of accessible β values determines the nature of the energy spectrum as being oscillator-like, rotor-like, etc.; a nucleus with a potential centered at $\beta = 0$ will possess an oscillator-like spectrum even if its expectation value for the deformation is large while a nucleus with a potential centered around a stiff, deformed $\beta \neq 0$ minimum will have a rotor-like spectrum even if its deformation is small. In a simple picture of a rigid rotor the magnitude of the deformation then controls directly the moment of inertia of the nucleus and hence the rotational energy scales. This is understandable if one realizes the direct link between the moment of inertia and the deformation (only the deformed surface layer is free to participate in rotation).

In transitional nuclei, a given nuclear eigenstate may have a probability distribution spanning a range of different deformations. Different nuclear observables are sensitive to different aspects of the onset of deformation. For example, for the stiff oscillator, the energy of the first excited 0^+ state is twice the energy of the first 2^+ state for small deformations, and both energies are quite high. As the potential becomes softer

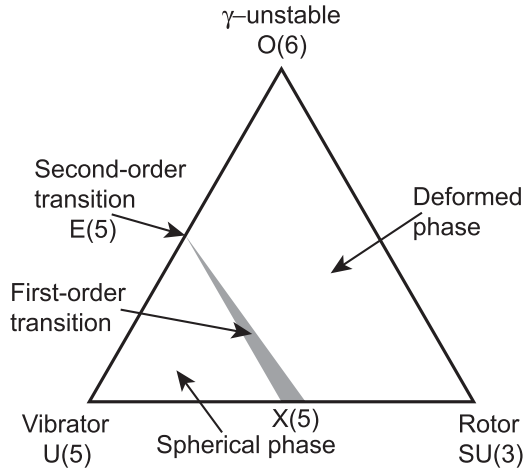

FIG. 1. Analytical benchmarks in the Casten triangle.

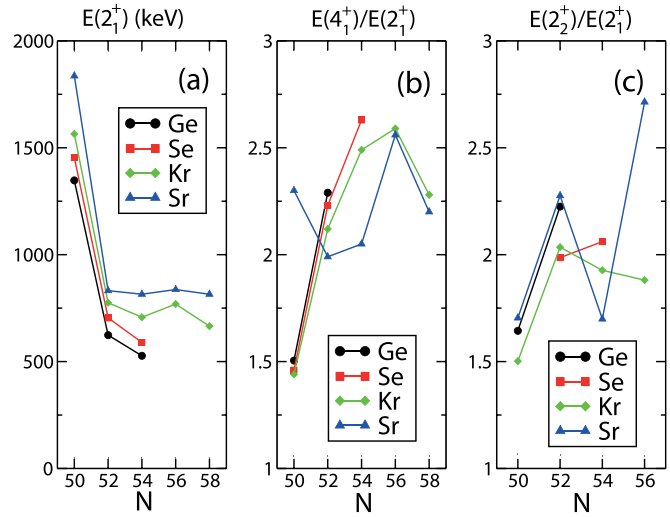

FIG. 2. Experimental energies of the 2_1^+ states and the energy ratios $E(4_1^+)/E(2_1^+)$, $E(2_2^+)/E(2_1^+)$ for Ge, Se, Kr, and Sr isotopes.

both energies decrease and some degree of anharmonicity is observed. With increasing deformation the energy of the first 2^+ state (changing its nature from a vibrational to a rotational) further decreases while the 0^+ state, retaining its vibrational character (evolving into a β-vibrational bandhead), increases its excitation energy.

Several theoretical ideas have been advanced regarding structural evolution in the transitional nuclei. Interacting boson model (IBM) studies, for example, have revealed that the transition from spherical to deformed structures has characteristics of a first- or second-order phase transition [2]. Empirical examinations of basic observables show that sharp discontinuities in behavior occur at a critical point along the transition.

An especially simple geometric description of nuclei near the critical point of the phase transition has been proposed by Iachello [3,4]. The deformation potential is expected to be relatively flat in β, allowing the nucleus to assume either a spherical or a deformed shape with minimal energy penalty. Such a flat-bottomed potential can be approximated by an infinite square-well potential in the deformation variable β, termed E(5), and describes a γ-soft transition. A square well with an additional stabilization in the γ degree of freedom termed X(5) is used for the description of axially symmetric transitional nuclei. Thus, the E(5) and X(5) models provide analytical benchmarks for the interpretation of transitional nuclei as much as the structural limits described conveniently by the Casten triangle provide benchmarks for the interpretation of spherical or well-deformed nuclei (see Fig. 1).

Our aim in the present paper is first to show, starting from a purely collective ACM approach, that it is possible to characterize the selenium isotopes ^{86,88}Se as near-E(5) transitional between a spherical vibrator and a gamma-soft rotor. It will enable us to get a global perspective on their structure even if a perfect description of the excited states is not expected within this simple model. Then we will turn to the microscopic study of the structure of those isotopes within the constrained Skyrme and Gogny-Hartree-Fock method.

Our analysis will be based on the data obtained by thermal neutron-induced fission, reported in Ref. [5]. Recently, neutron-rich Se isotopes were studied via in-beam γ-ray spectroscopy and then analyzed theoretically with beyond-mean-field calculations based on the Gogny D1S interaction. This analysis suggests that both the triaxial degree of freedom and shape coexistence play important roles in the neutron-rich Se isotopes [6]. Similar results were obtained within the framework of the large-scale shell model, assuming ^{78}Ni as a core [7]. Large-scale shell-model calculations in the vicinity of ^{78}Ni have also been carried out in Ref. [8]. The calculation focused on ^{86}Ge and ^{88}Se, and predicted maximum triaxiality to appear in ^{86}Ge. This phenomenon has been explained within a pseudo-SU(3) symmetry framework.

II. SYSTEMATIC STUDY OF NUCLEI WITH $N = 50$–58

It order to put things in the right perspective it is useful to recall the experimental situation of nuclei in the neigborhood of ^{86,88}Se. In Fig. 2(a) the evolution of the energies of the excited 2_1^+ state in the Ge, Se, Kr, and Sr isotopes is shown. The excited 2_1^+ state in ^{88}Se lies at 589.4 keV, just between the corresponding energies for ^{86}Ge and ^{90}Kr. The 2_1^+ energies for each isotopic chain for $N = 52$–58 decrease as one passes from Sr ($Z = 38$) to Ge ($Z = 32$), indicating an evolution towards a stronger quadrupole deformation. The energy ratio $E(4_1^+)/E(2_1^+)$ [Fig. 2(b)] for $N = 52$ varies between 2 and 2.3, showing an evolution from a spherical vibrational to a transitional, γ-soft nucleus. For $N = 54$ this ratio increases to 2.5–2.6, typical for transitional nuclei. The degree of collectivity in each isotopic chain increases with increasing neutron number. This is reflected, for example, by increasing values of the reduced transition rates $B(E2; 2_1^+ \rightarrow 0_1^+)$ from about 10 to 20 W.u. when one passes from ^{88}Kr to ^{94}Kr [9–11].

The deformation parameter β was estimated to be 0.24(2) in ^{88}Ge. In the above work the empirical Raman formula, which associated the deformation parameter to $E(2_1^+)$, was used [12]. Using the same approach, $\beta = 0.22(2)$ was obtained for ^{88}Se. It should be noted that the ratio $R_{4/2} = E(4_1^+)/E(2_1^+) = 2.63$ for ^{88}Se, i.e., higher than for the

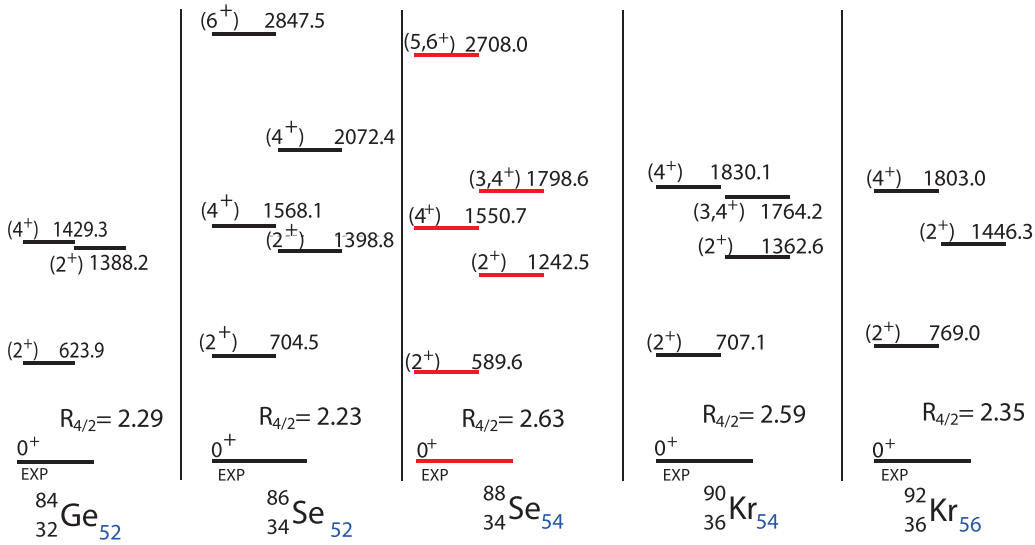

FIG. 3. Experimental spectra of ^{84}Ge, ^{86,88}Se, and ^{90,92}Kr.

neighboring nuclei, indicates a more rigid potential. A more pronounced rotational-like structure in the Se isotopes in comparison to Kr ($Z = 36$) and Sr ($Z = 38$) points towards a subshell closure at $Z = 38$. Moreover, Figs. 2(b) and 2(c) show that the $N = 54$ subshell has the most pronounced effect for the Sr nuclei.

The excited state $E(2_2^+)$ in ^{88}Se is one of the lowest in this mass region. It lies below the corresponding $E(4_1^+)$ state, indicating a large degree of γ softness or triaxiality. The ratios $E(2_2^+)/E(2_1^+)$ are shown in Fig. 2(c). A comparison of excitation energies of nuclei in this mass region also reveals a lot of similarities (see Fig. 3). The energies $E(2_1^+)$, $E(4_1^+)$, and $E(2_2^+)$ are about the same in ^{84}Ge, ^{86,88}Se, and ^{90,92}Kr. The energy difference $E(4_1^+) - E(2_2^+)$ is almost the same in ^{86,88}Se and ^{90,92}Kr, pointing towards a similar deformation of those nuclei. In ^{84}Ge, the $E(4_1^+)$ and $E(2_2^+)$ energies are almost degenerate, a result compatible with a complete γ softness in the Wilets-Jean (WJ) limit of the Bohr collective model (BM) [13]. This does not necessarily mean that the WJ limit of the BM is perfectly suitable for the description of these nuclei, but it indicates that a pronounced γ softness of the potential should be assumed for the shape of those nuclei and that the character of the shape transition may be close to E(5), a limit appropriate to the γ-soft transition.

III. ALGEBRAIC COLLECTIVE MODEL

The ACM, introduced as a computationally tractable version of the BM [13] restricted to rotational and quadrupole vibrational degrees of freedom, is characterized by a well defined algebraic structure. Unlike the conventional U(5) ⊃ SO(5) ⊃ SO(3) dynamical subgroup chain used, for example, in the Frankfurt group program [14,15], the ACM makes use of the subgroup chain

$$\mathrm{SU}(1,1) \times \mathrm{SO}(5) \supset \mathrm{U}(1) \times \mathrm{SO}(3) \supset \mathrm{SO}(2) \qquad (1)$$

to define basis wave functions as products of β wave functions and SO(5) spherical harmonics. Several advantages result from this choice of dynamical subgroup chain: (i) with the now available SO(5) Clebsch-Gordan coefficients [16,17], and explicit expressions for SO(5) reduced matrix elements, matrix elements of BM operators can be calculated analytically; (ii) by appropriate choices of SU(1,1) modified oscillator representations, the β basis wave functions range from those of the U(5) ⊃ SO(5) harmonic vibrational model to those of the rigid-β wave function of the SO(5)-invariant WJ model; and (iii) with these SU(1,1) representations, collective model calculations converge an order of magnitude more rapidly for deformed nuclei than in the U(5) ⊃ SO(5) bases. Thus, the ACM combines the advantages of the BM and the IBM and makes collective model calculations a simple, routine procedure [1,18–20].

A detailed description of the ACM can be found in Ref. [1]. A general purpose ACM Hamiltonian is given, for example, in the form

$$\hat{H}(M,\alpha,\kappa,\chi) = \frac{-\nabla^2}{2M} + \frac{1}{2}M[(1-2\alpha)\beta^2 + \alpha\beta^4] - \chi\beta\cos 3\gamma + \kappa\cos^2 3\gamma, \qquad (2)$$

where

$$\nabla^2 = \frac{1}{\beta^4}\frac{\partial}{\partial\beta}\beta^4\frac{\partial}{\partial\beta} + \frac{1}{\beta^2}\hat{\Lambda} \qquad (3)$$

is the Laplacian on the five-dimensional collective model space and $\hat{\Lambda}$ is the SO(5) angular momentum operator [21]. Such a Hamiltonian, expressed in terms of the quadrupole deformation parameters β and γ, serves as a useful starting point for a description of a wide range of nuclear collective spectra.

The terms β^2 and $\cos 3\gamma$ in Eq. (2) are defined in terms of the quadrupole tensor operator $\hat{Q}$ by

$$\hat{Q}\cdot\hat{Q} = \beta^2, \quad (\hat{Q}\otimes\hat{Q}\otimes\hat{Q})_0 = -\sqrt{\frac{2}{35}}\beta^3\cos 3\gamma. \qquad (4)$$

The last term in the Hamiltonian (2), proportional to $\cos^2 3\gamma$, can induce a triaxial minimum of the potential. A

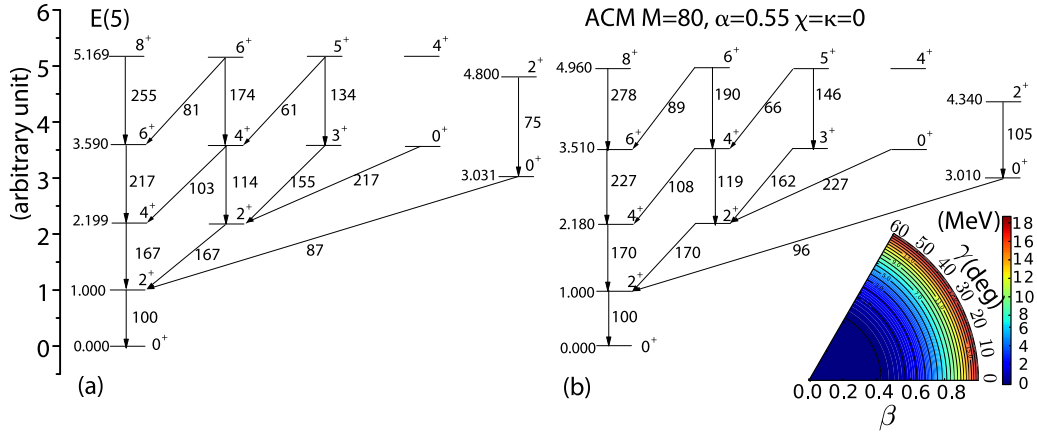

FIG. 4. E(5) spectrum and its ACM counterpart. The B($E2$) transition rates are shown as percentages of that for the $2_1^+ \rightarrow 0_1^+$ transition.

delicate competition between all the terms in the potential and the last two terms in particular will determine whether the potential energy minimum will remain axially symmetric (the term proportional to $\cos 3\gamma$ dominates) or will be driven to a triaxial minimum by the last term.

It should be noted that the prolate-to-oblate transition is obtained trivially by changing the sign of the parameter χ, and this sign change does not produce any effect on the calculated spectra as the Hamiltonian (2) is isospectral with regard to this sign transformation.

In their study of the second-order phase transition from a spherical vibrator to a gamma-soft rotor, Turner and Rowe have used a simplified approach containing only two variable parameters [22]: an effective mass parameter M and a control parameter α. The control parameter is such that when $\alpha = 0$ the Hamiltonian is that of a spherical vibrator, and when α is large it approaches that of an adiabatically decoupled rotor-vibrator. They have shown that the range of α in which the low-energy states of the model are in a transition region, between that of a harmonic spherical oscillator (small α) and that of an adiabatic rotor-vibator (large α), shrinks as M increases, and as $M \rightarrow \infty$ a critical point develops at $\alpha = 0.5$, at which the coefficient of the β^2 term vanishes.

The main purpose of this part of the analysis is first to see how the analytical E(5) limit can be approached within the ACM and then to position our nuclei in the transition region between the spherical and the deformed phase by choosing appropriate values of the ACM parameters. This will enable us to characterize the type of the transition realized in the nuclei studied.

IV. NUMERICAL RESULTS OBTAINED WITHIN THE ACM

As discussed in the above paragraphs, a γ-soft potential seems to be the most appropriate one for ^{86,88}Se. The limiting situation with a γ independent potential can be characterized by special symmetry properties. The Hamiltonian consisting of a γ-independent potential and the harmonic kinetic energy operator is invariant under the group O(5) of rotations in the five-dimensional space of shape parameters $\alpha_{2\mu}$. As a consequence, the energy levels follow a multiplet structure and the wave functions are products of radial and angular parts. It is of interest to see to what extent, and for what parameters, E(5)-like behavior can be reproduced with the ACM. We show in Fig. 4(a) the level energies and $B(E2)$ strengths in E(5), normalized to $E(2_1^+)$ and $B(E2; 2_1^+ \rightarrow 0_1^+)$, respectively. The ACM counterpart of the E(5) spectrum is shown in Fig. 4(b). We observe that the E(5)-like spectrum is best approximated using ACM parameters with near-critical values of $\alpha = 0.55$, $\chi = 0$, and $\kappa = 0$. This choice of parameters corresponds to a completely γ-independent potential. A very good agreement with the E(5) limit is obtained for energies and transition rates in the low-energy part of the spectrum.

The ACM calculation is compared to the experimental spectrum of ^{86}Se in Fig. 5 [5]. We observe that the experimental spectrum of ^{86}Se [Fig. 5(a)] contains a lot of characteristics typical for the E(5) limit. The $R_{4/2}$ ratio is 2.23, close to the E(5) 2.199 value. The ratio of $E(2_2^+)$ and $E(2_1^+)$ energies of 1.986 is also close to its E(5) counterpart of 2.199. Other E(5)-like properties of ^{86}Se are the near degeneracy of $E(2_2^+)$ and $E(4_1^+)$. The energies of the observed $E(4_2^+)$ and $E(6_1^+)$ states (2072.4 and 2847.5 keV, respectively) are also in a reasonable agreement with the E(5)-like values. Most of the above features of the ^{86}Se spectrum are reproduced by the ACM [Fig. 5(b)]. The drawback of the ACM calculations with very soft potentials is a large centrifugal stretching reflected

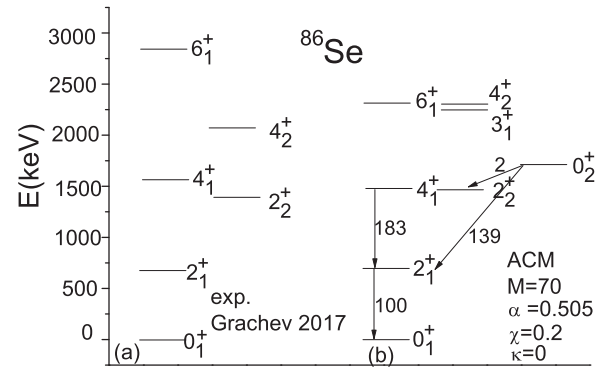

FIG. 5. Experimental spectrum of ^{86}Se (Grachev 2017 [5]) and its ACM counterpart. The $B(E2)$ transition rates are shown as percentages of that for the $2_1^+ \rightarrow 0_1^+$ transition.

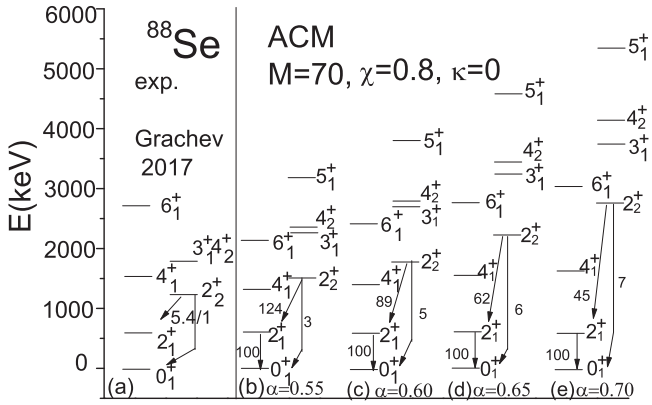

FIG. 6. Experimental spectrum of ^{88}Se (Grachev 2017 [5]) as compared with different ACM spectra obtained with the parameters $\alpha = 0.55, 0.60, 0.65$, and 0.70. The $B(E2)$ transition rates are shown as percentages of that for the $2_1^+ \rightarrow 0_1^+$ transition.

by low ground-band energies, an effect that becomes more pronounced with increasing spin.

The experimental spectrum of ^{88}Se, with two additional neutrons, resembles more a perturbed E(5) limit, or a mixture of the E(5) and X(5) limits [see Fig. 6(a)]. The $R_{4/2}$ ratio of 2.63 is closer to the X(5) value of 2.904, and is consistent with increasing β deformation with an increasing number of valence neutrons. On the other hand the E(5)-like γ softness of the potential, reflected by a small ratio of $E(2_2^+)$ and $E(2_1^+)$ energies of 2.1, persists. That contrasts with the X(5) limit where the 2_2^+ state is a member of the first excited β band and is located at 7.45 times the energy of the 2_1^+ state.

The experimental ratio $R_2 = B(E2; 2_2^+ \rightarrow 2_1^+)/B(E2; 2_2^+ \rightarrow 0_1^+) = 5.4(2.0)$ in ^{88}Se has been obtained from the measured γ-ray branching ratio [5]. It is close to the X(5) value of 3.9. [Note that the $B(E2; 2_2^+ \rightarrow 0_1^+)$ value is exactly zero in the E(5) limit and that nonzero values arise and increase with an increasing χ parameter]. The ACM value of R_2 changes rapidly near the critical point $\alpha = 0.5$. Optimizing both the energies and R_2 with a single set of ACM parameters turns out to be difficult. As the results are the most sensitive to the parameter α, we made a qualitative calculation by varying only this parameter between the values 0.55 and 0.7 [see Figs. 6(b)–6(e). Smaller values of α favor low $E(2_2^+)$ and larger R_2. When a larger value of α, close to 0.7, is taken, $E(2_2^+)$ increases while R_2 drops down to the experimental value. Even though all the known properties of ^{88}Se are not successfully described with a single set of ACM parameters, it is clearly seen that the parameter α remains close to its critical value of 0.5. The parameter χ is slightly larger than that for ^{86}Se, indicating a larger departure from the E(5) limit.

It should be noted that the value of the ratio $R_2 = B(E2; 2_2^+ \rightarrow 2_1^+)/B(E2; 2_2^+ \rightarrow 0_1^+)$ reported in Ref. [6] is 24(4). There may be several reasons for the difference in comparison with our result. First, the EXILL data reported in Ref. [5] may have a stronger population of the yrast band while the RIKEN data reported in Ref. [6] may populate the γ band more strongly. RIKEN data present broad, flat peaks on a high background while in the EXILL data some contamination in the gates may have made the selection less precise. Thus, it is difficult to make a decision of which of those two experimental values is better. Of course, a large value of R_2 speaks in favor of an almost γ-independent potential [in the case of complete γ independence the transition $B(E2; 2_2^+ \rightarrow 0_1^+)$ relating two states with the seniority quantum number difference $\Delta v = 2$ is identically zero]. However, a better quantitative estimate of this ratio would be needed to draw definite conclusions.

Moreover, calculations in Refs. [6,8] predicted 0_2^+ states in neutron-rich Se isotopes connected strongly to the 2_2^+ states, which would favor the WJ interpretation of these nuclei. Again, the transition $B(E2; 0_2^+ \rightarrow 2_1^+)$ connecting $\Delta v = 2$ states is identically zero in this limit.

The ACM result is somewhat different. The 0_2^+ state in ^{86}Se is predicted at about 1700 keV (see Fig. 5), in an impressive agreement with the experimental trends (the observed 0_2^+ energies vary between 1 and 2 MeV from ^{68}Se to ^{84}Se). However, the dominant decay of this 0_2^+ state is to the 2_1^+ state. This result is in agreement with the decay pattern of the observed 0_2^+ states in the lighter Se isotopes and would favor the E(5)-like interpretation of this nucleus.

It should be noted that the energy of the 0_2^+ state depends sensitively on the parameter α, rising sharply and rapidly with increasing α. For the values of α used to study ^{88}Se in Fig. 6, the 0_2^+ energy varies between 1.7 MeV (for $\alpha = 0.55$) to about 4 MeV (for $\alpha = 0.7$). Its decay pattern also changes rapidly as a function of α, the dominant decay being into the 2_1^+ state for smaller α and into 2_2^+ one for larger α. The experimental energy of 0_2^+ in ^{88}Se is not known. However, if one assumes it to be close to the 0_2^+ energies in lighter Se isotopes (between 1 and 2 MeV), a smaller value of α would be more appropriate. A smaller value of α would then favor a larger $R_2 = B(E2; 2_2^+ \rightarrow 2_1^+)/B(E2; 2_2^+ \rightarrow 0_1^+)$ ratio (see Fig. 6).

Indeed, the energy and the decay patern of the 0_2^+ state may be used as a very strong indicator of the E(5)-like behavior. Moreover the energies predicted by the ACM (if smaller values of α are used) are reasonably close to its E(5)-like value $[E(0_2^+)/E(2_1^+) = 3.031]$.

It is interesting to observe the rapid changes of nuclear structure properties near the critical point $\alpha = 0.5$. We show in Fig. 7 the behavior of the excitation energies of the 4_1^+, 4_2^+, 2_2^+, and 3_1^+ states. They all approach their experimental values for α near the critical value of 0.5.

In conclusion, a perfect ACM description of ^{86,88}Se is beyond the reach of the model. However, the ACM analysis shows that ^{86}Se bears a lot of properties expected for an E(5) transitional nucleus, but more experimental data are needed to make a more definitive conclusion. By increasing the number of neutrons, the deformation stabilizes in ^{88}Se and the E(5) symmetry is more perturbed. Due to the small parameter χ, the resulting potential is still very γ soft.

Having localized ^{86,88}Se in the Casten triangle as transitional nuclei near the E(5) transitional point, we will now turn to the microscopic study of the structure of these nuclei to ascertain the degree of collectivity on more fundamental grounds. First we investigate ground-state deformations in the framework of the constrained Skyrme Hartree Fock

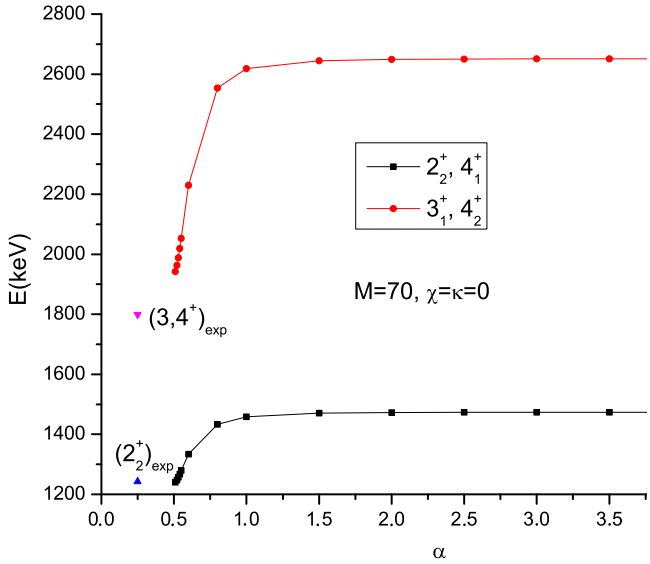

FIG. 7. ACM energies of the 2^+_2 (4^+_1) and 3^+_1 (4^+_2) states as a function of the parameter α

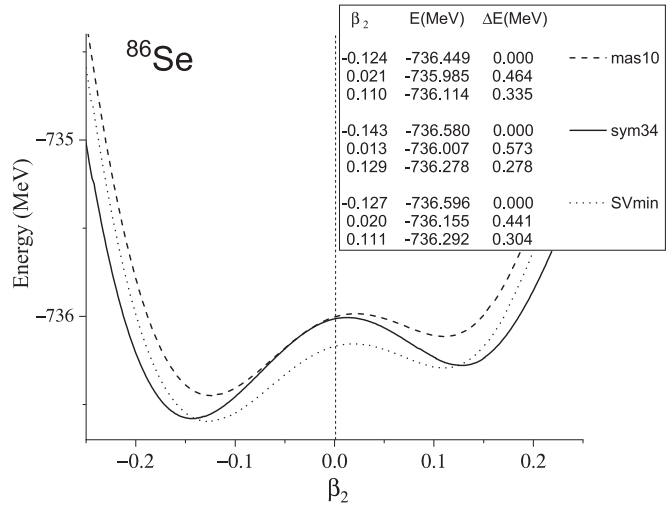

FIG. 8. PEC as a function of β_2 for ^{86}Se. The calculated SHF potential energies E and energy differences ΔE between the oblate and prolate minima and the barrier heights are listed in the frame.

model, then we focus on the structure of the ground-state and low-lying states within the framework of the symmetry conserving configuration mixing method with Gogny energy density functionals.

V. SKYRME HARTREE-FOCK CALCULATIONS

Among self-consistent mean-field methods, the Skyrme-Hartree-Fock model (SHF) is the most widely used [23] and represents another possibility to investigate nuclear ground state (g.s.) properties. Pioneering calculations exploring the energy of the nucleus as a function of quadrupole deformation parameters using self-consistent microscopic theories have been carried within the Skyrme functional in Ref. [24], for the Gogny functional in Ref. [25], and within the relativistic mean-field approximation in Refs. [26,27].

There are plenty of SHF functional parametrizations available in the literature. We refer here to a recent family of parametrizations which was derived from least-square fitting of its free parameters to a large pool of selected g.s. observables and, optionally, other nuclear properties [28]. This family includes an optimization to ground state properties only, denoted SV-min, and a couple of related parametrizations with dedicated variation of nuclear matter properties (incompressibility, symmetry energy, effective isoscalar, and isovector mass) [28]. We have checked all of them for the present test cases, and in addition three older choices, namely Sk-M*, SLy6, and SkI3. For presentation we confine that selection to a few parametrizations, namely SV-min as unconstrained optimum, SV-bas as base point for dedicated variation of nuclear matter properties (in practice, similar to SV-min), SV-sym34 with symmetry energy $J = 34$ MeV, and SV-mas10 with isoscalar effective mass $m^*/m = 1$. These four forces do not contain the tensor spin-orbit term. To check its impact, we also consider the parametrization SV-tls, which is fitted exactly the same way as SV-min but with tensor spin-orbit included. All these parametrizations reproduce rather well the binding energies of ^{86}Se and ^{88}Se, 738.04 and 747.56 MeV [29], respectively (note that these soft nuclei would gain a bit more energy by vibrational ground state correlations). In calculations using the axial SHF code SKYAX with a density-dependent δ-force interaction in the pairing channel [30], single-particle levels up to 75 MeV were taken into account (eight oscillator shells).

In the O(6) or WJ limit one would expect to observe a typical double-well structure of prolate and oblate minima ($\pm\beta_2$) separated by an energy barrier at zero deformation in the SHF potential energy curve (PEC) calculations as a function of the quadrupole deformation parameter β_2. Along the path towards the E(5) limit the barrier gets lower and the PEC becomes flatter. Results are presented in Fig. 8 (^{86}Se) and Fig. 9 (^{88}Se). Both nuclei exhibit zero octupole and small positive hexadecapole deformations. A relatively flat PEC with symmetric oblate-prolate minima (energy difference ≈0.3 MeV, barrier height ≈0.5 MeV) is characteristic for ^{86}Se that seems to be closer to the E(5) limit, whereas for ^{88}Se the energy difference between the oblate and prolate minima gets lower (≈0.2 MeV) and the barrier get higher and is more SHF parametrization dependent (≈0.6–1.4 MeV).

Phase transitions along the chain of selenium isotopes are illustrated in Figs. 10 and 11 for two parametrizations, namely the g.s. binding energy minimizing one, SV-sym34, and the variation base point one, SV-bas [28]. Here we show oblate and prolate deformation minima, $\beta_{2\min} < 0$ and $\beta_{2\min} > 0$, respectively, and deformation energies defined as $E(\beta_{2\min} < 0) - E(\beta_2 = 0)$ and $E(\beta_{2\min} > 0) - E(\beta_2 = 0)$ along the chain of Se isotopes ($N = 40$–66) for the SV-bas and SV-sym34 parametrizations. The triaxiality, computed according to Ref. [31], is also shown for nonspherical isotopes, where it is well defined. The triaxiality develops only in the vicinity of the spherical nucleus ^{84}Se, where oblate and prolate minima are almost degenerate. Below the closed neutron shell

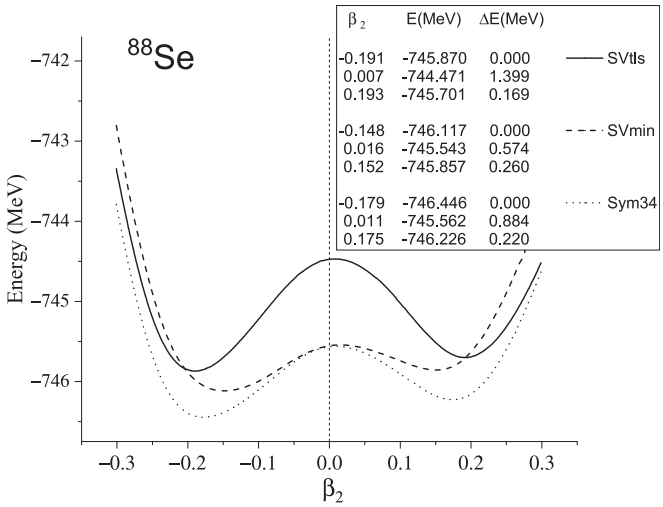

FIG. 9. PEC as a function of β_2 for ^{88}Se. E and ΔE are the same quantities as in Fig. 8.

$44 < N < 50$, prolate shapes with small $\beta_2 \approx 0.1$ are preferred, whereas for $N > 56$ the oblate deformation stabilizes in the ground state. It is noteworthy that all parametrizations deliver very similar PECs; however, with interesting differences in detail. The largest effect is seen for SV-tls, where the switch to tensor spin-orbit coupling has enhanced the barrier between prolate and oblate minima. This is, although somewhat unexpected, plausible because barriers are produced by shell effects and these are sensitive to the spin-orbit splitting.

To find the energies of the lowest 2^+ states, the results of the quadrupole-constrained calculations for the two selected SHF parametrizations were further processed in the generator coordinate method (GCM) at the level of the Gaussian overlap approximation [32]. Both parametrizations give similar behavior along the studied chain of selenium isotopes: a correlated decrease of 2^+ energies with increasing quadrupole deformation (see Fig. 12). In particular, for ^{86}Se and ^{88}Se they well reproduce the experimental 2_1^+ energies (the experimental energy of the 2_1^+ state in $^{74-82}$Se isotopes is about 600 keV; it rises to 1455 keV in ^{84}Se isotope and drops to 704 and 590 keV in ^{86}Se and ^{88}Se isotopes, respectively.)

VI. SYMMETRY CONSERVING CONFIGURATION MIXING CALCULATIONS

We now discuss the most microscopic approach used in this work to study the structure of $^{86-88}$Se isotopes, namely, the symmetry conserving configuration mixing (SCCM) method with Gogny energy density functionals (EDF) [6,8,33,34]. The nuclear states given by the SCCM method are obtained by building first a set of Hartree-Fock-Bogoliubov (HFB) wave functions with different axial and nonaxial quadrupole deformations, (β_2, γ). These intrinsic wave functions are found using the particle-number variation after projection (PN-VAP) method with constraints on the quadrupole operators. This procedure is superior to plain HFB calculations because it can handle pairing correlations much better. Then, the set of intrinsic wave functions is projected onto good particle numbers and angular momentum to restore the symmetries broken by the HFB states. The final step is the configuration (shape) mixing within the GCM framework without assuming any Gaussian overlap approximation. Hence, the energy spectrum, electromagnetic moments and transition probabilities, and the so-called collective wave functions are finally obtained from solving the Hill-Wheeler-Griffin equations associated with the mixing of the projected HFB-like states described above. A detailed description of the SCCM method can be found in Refs. [33,34] and references therein. The present SCCM calculations have been performed with the Gogny D1S two-body interaction [35]. The results have been partially reported in Refs. [6,8] but a more detailed description of the structure of $^{86-88}$Se will be given below.

A first insight into the structure of the nuclei ^{86,88}Se is the study of the particle number projected energy as a function of the quadrupole deformation, (β_2, γ), shown in Fig. 13. These potential energy surfaces (PESs) are the natural extension to the triaxial degree of freedom of the PEC discussed in the previous section, but now they are computed with the Gogny

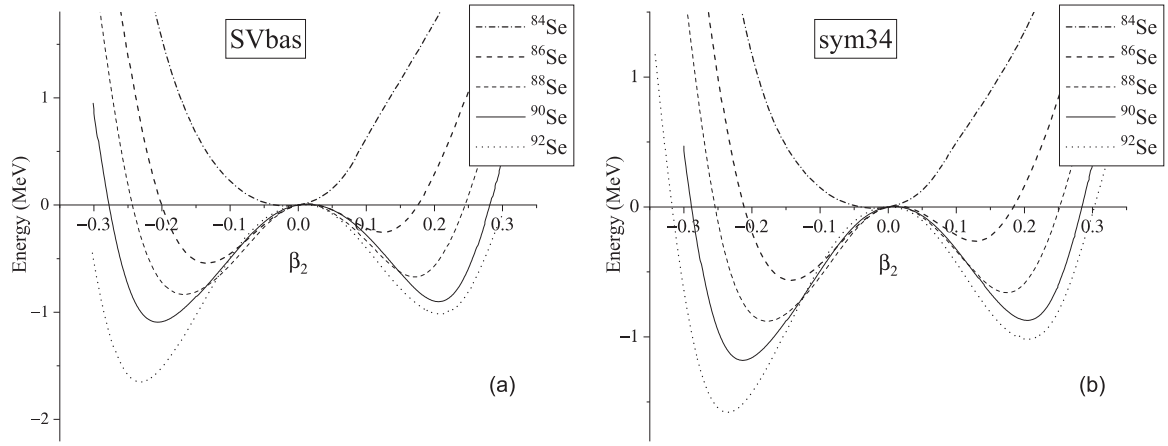

FIG. 10. PECs as functions of β_2 for the chain of isotopes $^{84-92}$Se for two SHF parametrizations, SVbas (a) and sym34 (b).

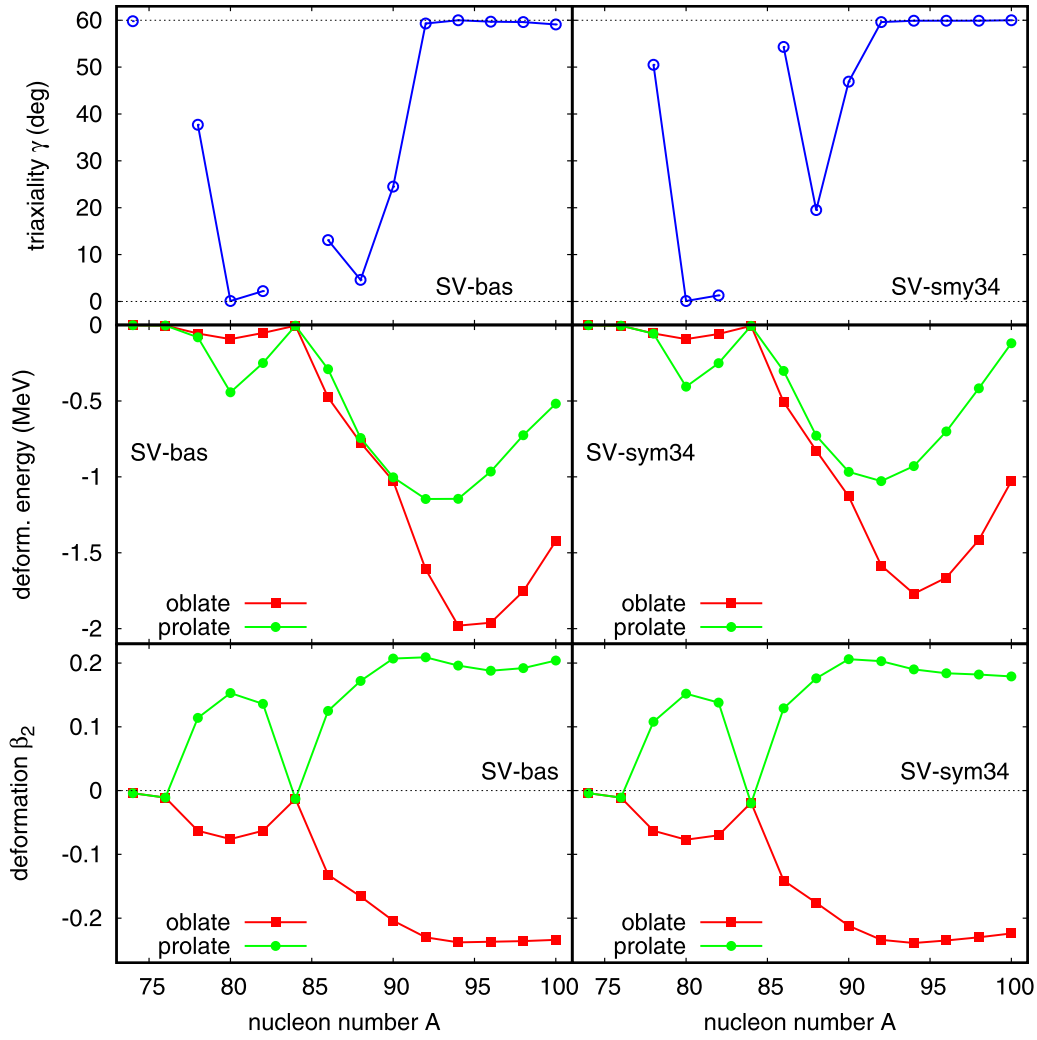

FIG. 11. Triaxiality, oblate and prolate PEC minima, and corresponding deformations β_2 for two SHF parametrizations for isotopes of Se.

D1S interaction and include the effect of particle number symmetry restoration. We observe that both isotopes show a rather flat PES around $\beta_2 \approx 0.20$ along the γ degree of freedom. The γ softness is larger in ^{86}Se and the absolute minimum for this nucleus is found at an oblate ($\gamma = 60^\circ$) configuration. For ^{88}Se the PES evolves towards a prolate minimum at $\beta_2 \approx 0.20$.

From these PESs one could expect that the triaxial degree of freedom will play a relevant role in the structure of the nuclear states. The next step in the SCCM method consists

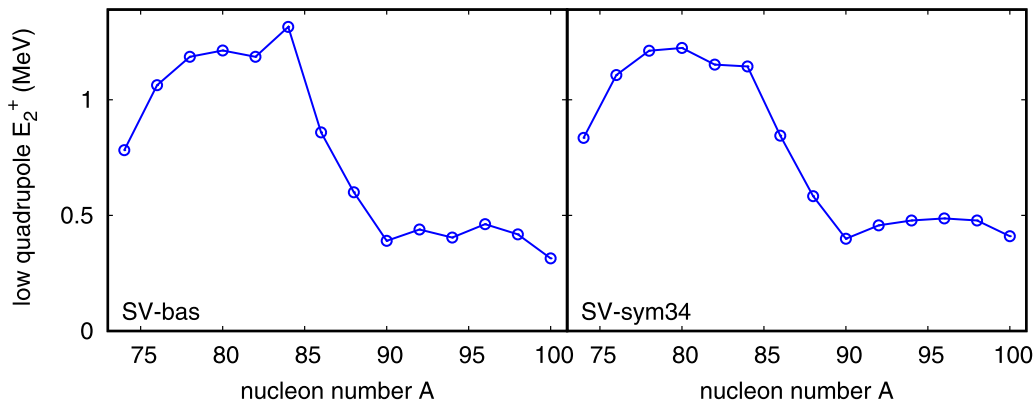

FIG. 12. Calculated energies of the first 2^+ states for two SHF parametrizations for isotopes of Se.

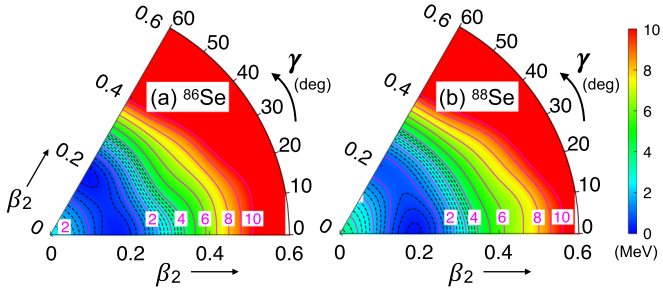

FIG. 13. Particle-number projected energy surfaces obtained with the Gogny D1S interaction in the (β_2, γ) plane for (a) ^{86}Se and (b) ^{88}Se isotopes.

TABLE I. Different ratios of excitation energies and transition probabilities calculated from experimental and theoretical values for ^{86}Se (left) and ^{88}Se (right). The definitions of these ratios are $R_{4/2} = E(4_1^+)/E(2_1^+)$, $R_{2/2} = E(2_2^+)/E(2_1^+)$, $R_{0/2} = E(0_2^+)/E(2_1^+)$, $R_{4/6} = E(4_2^+)/E(6_1^+)$, and $R_2 = B(E2, 2_2^+ \to 2_1^+)/B(E2, 2_2^+ \to 0_1^+)$.

	^{86}Se			^{88}Se			E(5)
	Expt.	SCCM	SM [36]	Expt.	SCCM	SM [36]	
$R_{4/2}$	2.226	2.467	1.885	2.674	2.614	2.600	2.199
$R_{2/2}$	1.761	1.915	2.026	2.124	1.989	2.290	2.199
$R_{0/2}$		2.029			2.165		3.031
$R_{4/6}$	0.728	0.727	0.801		0.729	0.702	1.000
R_2		510	5.5	24	54	3	∞

of the simultaneous particle number and angular momentum restoration of the states used to evaluate the energies shown in Fig. 13. Then, the mixing of these projected states is performed and the final spectrum, electromagnetic properties, and collective wave functions for each individual nuclear state are found. In Fig. 14 the excitation energies computed for ^{86}Se and ^{88}Se are represented. The states are sorted out in bands by grouping the states connected with the largest $B(E2)$ values. However, some states belonging to different bands are also connected with large electromagnetic transitions, as we will show below.

Some similarities are found in the spectra of the two isotopes studied here. Hence, three bands can be identified for both nuclei: (a) a ground state band with $\Delta J = 2$ that reveals some fingerprints of γ softness and/or triaxial rotation ($R_{4/2} = 2.47$ and 2.61 for ^{86}Se and ^{88}Se, respectively); (b) a first excited band with $\Delta J = 2$ where the 2_2^+ is slightly below the 0_2^+ state; and (c) a band with $\Delta J = 1$ with a 3_1^+ bandhead and the corresponding 2^+ state almost degenerate. The latter band cannot be associated with a γ band due to its different ordering of the lowest levels and a strong $K = 0, 2$ mixing obtained for those states in the calculations (see also Ref. [8]). Therefore, these nuclei cannot be interpreted as completely degenerate γ-soft [O(6)] or pure triaxial rotors (WJ model) since in those cases a band with the sequence $2^+, 3^+, 4^+, 5^+, \ldots$ can be unambiguously identified. Additionally, a well-defined rotational band with $\Delta J = 2$ is observed in ^{86}Se with a 0_3^+ bandhead. Apart from the $R_{4/2}$ ratio mentioned above, other experimental and theoretical ratios are shown in Table I. The table shows also the shell-model results obtained in Ref. [36]. Here we observe rather good agreement between the SCCM and experimental results. In addition a strong $B(E2, 0_2^+ \to 2_2^+)$ transition is obtained for both isotopes (2112 and 1957 e^2fm^4 for ^{86}Se and ^{88}Se respectively).

To shed more light on the quadrupole properties of these bands we analyze the collective wave functions for ^{86}Se

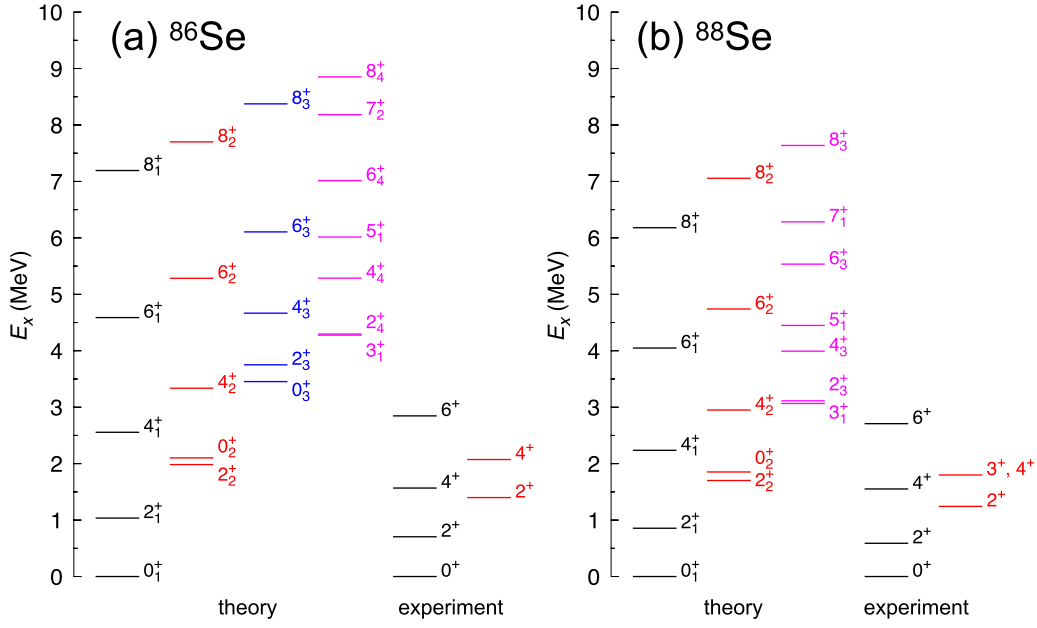

FIG. 14. Excitation energies computed with the SCCM method with the Gogny D1S interaction for (a) ^{86}Se and (b) ^{88}Se isotopes. Experimental values are also shown.

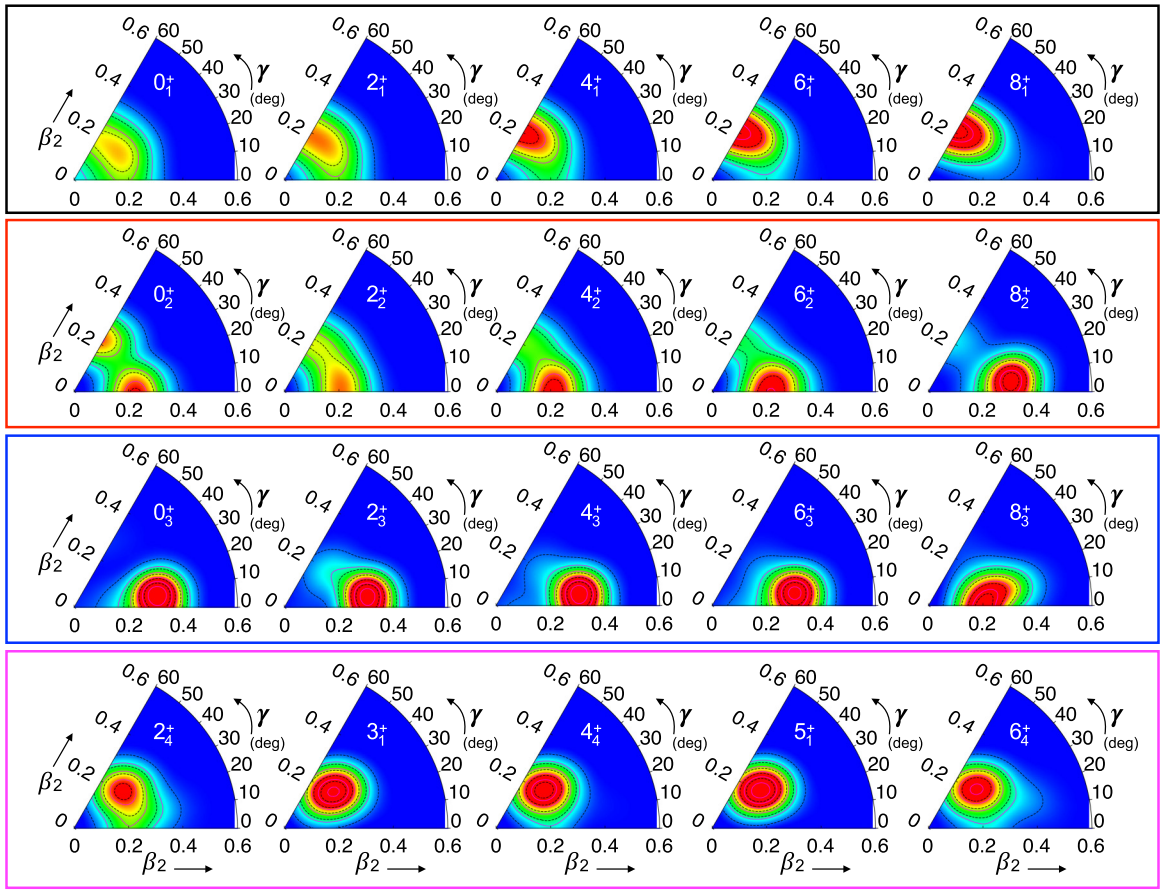

FIG. 15. Collective wave functions calculated for ^{86}Se. The colors of the boxes correspond to the colors of the bands shown in Fig. 14.

(^{88}Se) in Fig. 15 (Fig. 16). These functions represent the relative weight of the different deformations in each nuclear state. Hence, the ground state (g.s., 0_1^+) of ^{86}Se is a mixture of deformations in the γ direction and in an interval of $\beta_2 \in (0.15\text{–}0.25)$. Nevertheless, the largest contributions are located in the triaxial-oblate part of the (β_2, γ) plane. The shape of the collective wave functions of the g.s. band evolves towards pure axial oblate configurations ($\gamma = 60^\circ$) and $\beta_2 \approx 0.20$ when the angular momentum is increased. On the other hand, the first 0_2^+ excited state is a mixture of prolate and oblate configurations with a value of β_2 similar to the value obtained for the g.s. deformation. Here, two maxima are found at $\beta_2 \approx 0.2$ and $\gamma = 0^\circ$ (prolate) and 60° (oblate). Between these two maxima, along the γ direction, a minimum is obtained at $\gamma \approx 30^\circ$. This minimum is in fact located at the same deformation of the maximum observed in the g.s. collective wave function (0_1^+). Therefore, this structure can be interpreted as a vibration of the ground state along the γ degree of freedom. Then, the rest of the members of the first excited band evolve towards an axial prolate deformation with $\beta_2 \approx 0.20$. In addition, a well-defined rotational band is obtained on top of the 0_3^+ state with a slightly triaxial-prolate character ($\beta_2 \approx 0.30, \gamma \approx 10^\circ$). The collective wave functions of this band are rather constant from 0_3^+ to 6_3^+ and a band crossing is observed for the states $8_{2,3}^+$. Furthermore, the nucleus ^{86}Se shows the aforementioned $\Delta J = 1$ band with a triaxial character ($\beta_2 \approx 0.20, \gamma \approx 40^\circ$). The overlaps between the different states belonging to different bands can explain the large interband $B(E2)$ transitions obtained in the calculations. For example, the ground-state band is connected to the first and third excited bands through relatively large $4_2^+ \to 4_1^+, 6_2^+ \to 6_1^+, 3_1^+ \to 4_1^+$, and $5_1^+ \to 6_1^+$ transitions, and it is not mixed with the second excited rotational band. The first excited band members do have transitions to the second excited band ($2_3^+ \to 0_2^+$, $8_2^+ \to 6_3^+$, and $8_3^+ \to 6_2^+$) and to the third excited band ($2_4^+ \to 0_2^+$, $3_1^+ \to 2_2^+$, $5_1^+ \to 4_2^+$, and $4_4^+ \to 4_2^+$). Finally, the second and third excited bands are also connected through the transition $2_4^+ \to 0_3^+$.

Concerning the nucleus ^{88}Se, the range of relevant deformations is rather similar to the range discussed above for ^{86}Se, i.e., around $\beta_2 \approx 0.20$ (see Fig. 16). In this case, the ground state is more axial prolate deformed and the shape also evolves with increasing angular momentum. Hence, the 2_1^+ state is still prolate deformed but the maximum of the distribution moves towards larger values of γ in a smooth manner (with a rather constant $\beta_2 \approx 0.20$ value). The 0_2^+ state has a similar vibrational character as in ^{86}Se but now the 2_2^+ and 4_2^+ are oblate deformed. The evolution of the shapes of the collective wave functions in this band mirrors the evolution of the g.s. band, i.e., the 6_2^+ and 8_2^+ are now prolate

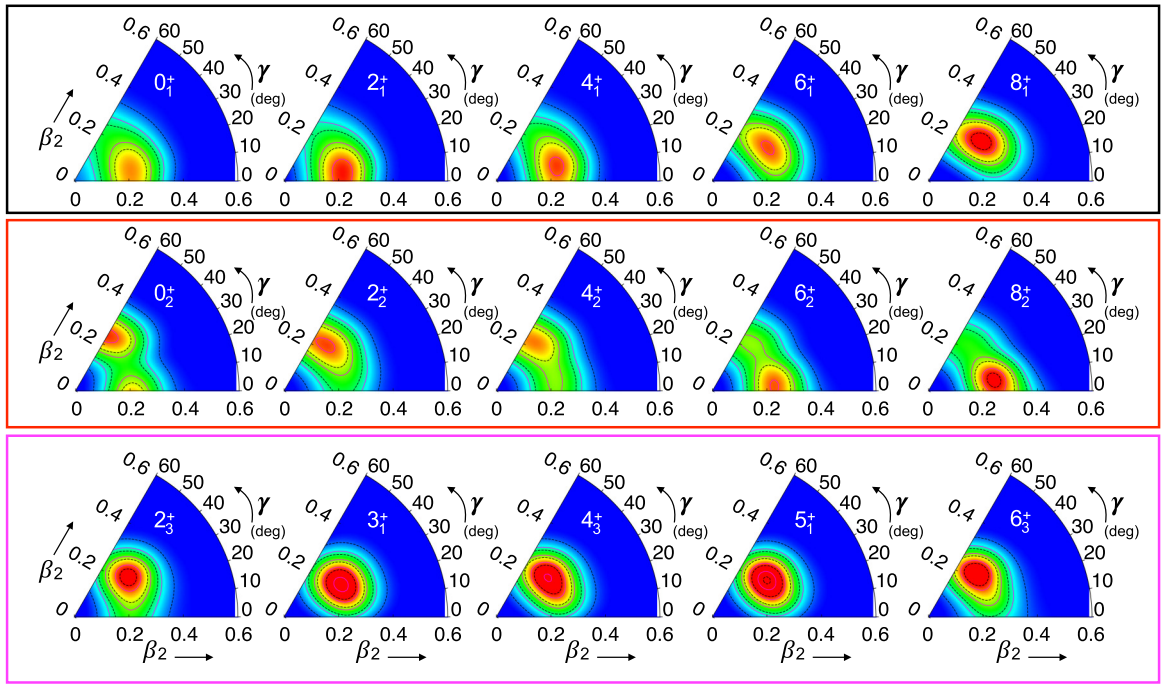

FIG. 16. Same as Fig. 15 but for ^{88}Se.

deformed with a non-negligible mixing with oblate shapes through the γ degree of freedom. Finally, the $\Delta J = 1$ band (second excited band) is rather similar to the one found in ^{86}Se. The most relevant interband transitions in this nucleus are $J_2^+ \to J_1^+$ ($J = 2, 4, 6, 8$) between states belonging to the g.s. and first excited bands; $2_3^+ \to 0_2^+$, $3_1^+ \to 2_2^+$, and $J_3^+ \to J_2^+$ ($J = 4, 6, 8$) between the first and second excited bands; and $5_1^+ \to 6_1^+$ between the g.s. and the second excited bands. We can see in Fig. 16 that the corresponding collective wave functions for these transitions have a non-negligible overlap. Complete results for in-band and interband reduced transition probabilities $B(E2)$ within the SCCM framework are shown in Table II. Experimentally only the values for $B(E2, 2_1^+ \to 0_1^+) = 438(^{+259}_{-171})$ and $B(E2, 4_1^+ \to 2_1^+) > 140\ e^2\text{fm}^4$ for ^{86}Se are known [7]. The theoretical predictions are in a rather good agreement with these values.

For ^{86}Se the shell-model calculations [7] indicate triaxiality for the yrast 0_1^+– 4_1^+ states, with intrinsic shape parameters $\beta \approx 0.2$ and $\gamma \approx 22^o$ and a fall to $\gamma = 12^o$ for the 6_1^+ state, whereas the SCCM predicts evolution towards an oblate shape. For ^{88}Se yrast bands 0_1^+– 6_1^+ higher deformation ($\beta \approx 0.25$) and lower $\gamma = 9^\circ$–14° were obtained in the shell model (SM). The SM predicts more deformed structure, better energy spacings and smaller transition rates between the yrast and excited bands. SCCM, on the other hand, predicts better ratios of excitation energies and transition probabilities (see Table I).

We finally remark the stretching of the SCCM energies with respect to the experimental values (see Fig. 14). This is a well known effect of the present implementation of the method, which tends to explore variationally better the ground state than the excited states. This drawback can be corrected by including time-reversal symmetry breaking HFB states through cranking calculations [37,38]. However, the computational cost of this improvement is very high [39] and

TABLE II. $B(E2, J_a^+ \to J_b^+)$ (in $e^2\text{fm}^4$) transition probabilities for intraband and inter-band transitions for ^{86}Se (top) and ^{88}Se (bottom) calculated with the SCCM method.

$J_a^+ \to J_b^+$	SCCM	$J_a^+ \to J_b^+$	SCCM
$2_1^+ \to 0_1^+$	548	$4_2^+ \to 4_1^+$	528
$4_1^+ \to 2_1^+$	797	$6_2^+ \to 6_1^+$	376
$6_1^+ \to 4_1^+$	917	$3_1^+ \to 4_1^+$	130
$8_1^+ \to 6_1^+$	1019	$5_1^+ \to 6_1^+$	119
$2_2^+ \to 0_2^+$	422	$2_3^+ \to 0_2^+$	84
$4_2^+ \to 2_2^+$	688	$8_2^+ \to 6_3^+$	572
$6_2^+ \to 4_2^+$	849	$8_3^+ \to 6_2^+$	163
$8_2^+ \to 6_2^+$	846	$2_4^+ \to 0_2^+$	92
$2_3^+ \to 0_3^+$	652	$3_1^+ \to 2_2^+$	317
$4_3^+ \to 2_3^+$	1036	$5_1^+ \to 4_4^+$	157
$6_3^+ \to 4_3^+$	1200	$5_1^+ \to 4_2^+$	109
$3_1^+ \to 2_4^+$	590	$4_4^+ \to 4_2^+$	172
$5_1^+ \to 3_1^+$	580	$2_4^+ \to 0_3^+$	183
$2_1^+ \to 0_1^+$	605	$4_3^+ \to 3_1^+$	663
$4_1^+ \to 2_1^+$	915	$5_1^+ \to 3_1^+$	561
$6_1^+ \to 4_1^+$	1083	$2_2^+ \to 2_1^+$	720
$8_1^+ \to 6_1^+$	1262	$4_2^+ \to 4_1^+$	543
$2_2^+ \to 0_2^+$	392	$6_2^+ \to 6_1^+$	432
$4_2^+ \to 2_2^+$	712	$8_2^+ \to 8_1^+$	266
$6_2^+ \to 4_2^+$	852	$2_3^+ \to 0_2^+$	233
$8_2^+ \to 6_2^+$	959	$3_1^+ \to 2_2^+$	482
$3_1^+ \to 2_3^+$	733	$4_3^+ \to 4_2^+$	322
$6_3^+ \to 5_1^+$	398	$6_3^+ \to 6_2^+$	278

we expect that the qualitative description of the nuclei under study will not change significantly.

VII. CONCLUSIONS

The ACM analysis of the isotopes ^{86,88}Se reveals that they are both characterized by very γ-soft potentials. The experimental spectrum of ^{86}Se [Fig. 5(a)] contains a lot of characteristics typical for the E(5) transitional limit. In ^{88}Se some of the properties of the ground-state band approach the X(5) ones; however, the E(5)-like γ softness of the potential persists. In particular, the $R_{4/2}$ ratio of 2.63 is closer to the X(5) value of 2.904. On the other hand the E(5)-like γ softness of the potential, reflected by a small ratio of $E(2_2^+)$ and $E(2_1^+)$ energies of 2.1, persists.

A very interesting link is found between the decay patterns of the 2_2^+ and the 0_2^+ states. A stronger decay of the 2_2^+ state into the 2_1^+ one reflected by a large ratio R_2 is obtained for smaller values of the parameter α. As a consequence, one would obtain a low-lying 0_2^+ state decaying predominantly to the 2_1^+ state. This behavior may be evidence of an E(5)-like nucleus. Somewhat larger values of α favoring a smaller ratio R_2 would lead to a dominant decay of 0_2^+ states to 2_2^+ states, as expected in the WJ limit.

The results obtained within the SHF approach are in qualitative agreement with the ACM analysis. A relatively flat PEC with symmetric oblate-prolate minima is characteristic for ^{86}Se that seems to be closer to the E(5) limit, whereas in ^{88}Se the energy difference between the oblate and prolate minima gets lower and the barrier gets higher and is more SHF parametrization dependent. Thus one can conclude that ^{86}Se is a better candidate for an E(5)-like nucleus than ^{88}Se. The calculations also reveal an interesting feature that the triaxiality develops only in the vicinity of the spherical nucleus ^{84}Se where oblate and prolate minima are almost degenerate.

Finally, the microscopic SCCM calculations with the Gogny D1S interaction display a more involved structure. Again, rather γ-soft PESs in the (β_2, γ) plane are found, being softer for ^{86}Se than for ^{88}Se. The results obtained after the symmetry restorations (particle number and angular momentum) and configuration mixing are in rather good agreement with the available experimental data, and some deviations from the E(5) and/or O(6) limits are predicted. In ^{86}Se a noticeable shape mixing along the γ degree of freedom is obtained for the ground state, and the rest of the states of this band evolve towards axial oblate configurations. On the other hand, the ground state of the nucleus ^{88}Se is mainly axially prolate deformed, and a transition from these prolate deformations to triaxial/oblate configurations is observed along the band when the angular momentum is increased. Additionally, the first 0_2^+ excited state can be interpreted as a vibration of the ground state along the γ direction in both isotopes. This state is slightly above the 2_2^+ state and strongly connected to it by $B(E2)$ transitions also in ^{86}Se and ^{88}Se, contrary to the E(5) limit. Finally, a $\Delta J = 1$ band is obtained with a 3_1^+ bandhead almost degenerated to a 2^+ state for both nuclei. The properties of this band are not the usual ones for a γ band and reveal a more involved structure than the predictions given by γ-soft, triaxial rotor, and/or critical point E(5) macroscopic models.

Therefore, knowledge of the properties of the 0_2^+ and the 3_1^+ states thus might be very helpful in determining whether or not ^{86}Se is a good candidate for an E(5)-like nucleus.

ACKNOWLEDGMENTS

This work was supported by the projects SP2018/84 and the National Programme for Sustainability I (2013-2020) financed by the state budget of the Czech Republic, identification code LO1406. G.T. acknowledges the financial support of the French-Czech LEA NuAG Collaboration. T.R.R. acknowledges the financial support of the Spanish MINECO under Contract No. FIS2014-53434-P and Programa Ramón y Cajal 2012 No. 11420.

[1] D. J. Rowe, T. A. Welsh, and M. A. Caprio, Phys. Rev. C. **79**, 054304 (2009).
[2] A. E. L. Dieperink, O. Scholten, and F. Iachello, Phys. Rev. Lett. **44**, 1747 (1980).
[3] F. Iachello, Phys. Rev. Lett. **85**, 3580 (2000).
[4] F. Iachello, Phys. Rev. Lett. **87**, 052502 (2001).
[5] I. N. Gratchev, G. S. Simpson, G. Thiamova, M. Ramdhane, K. Sieja, A. Blanc, M. Jentschel, U. Koster, P. Mutti, T. Soldner, G. deFrance, C. A. Ur, and W. Urban, Phys. Rev. C **95**, 051302 (2017).
[6] S. Chen *et al.*, Phys. Rev. C **95**, 041302(R) (2017).
[7] J. Litzinger *et al.*, Phys. Rev. C **92**, 064322 (2015).
[8] K. Sieja, T. R. Rodríguez, K. Kolos, and D. Verney, Phys. Rev. C **88**, 034327 (2013).
[9] D. Mucher *et al.*, Prog. Part. Nucl. Phys. **59**, 361 (2007).
[10] J. M. Regis, J. Jolie, N. Saed-Samii, N. Warr, M. Pfeiffer, A. Blanc, M. Jentschel, U. Koster, P. Mutti, T. Soldner, G.S. Simpson, F. Drouet, A. Vancraeyenest, G. deFrance, E. Clement, O. Stezowski, C. A. Ur, W. Urban, P. H. Regan, Z. Podolyak, C. Larijani, C. Townsley, R. Carroll, E. Wilson, L. M. Fraile, H. Mach, V. Paziy, B. Olaizola, V. Vedia, A. M. Bruce, O. J. Roberts, J. F. Smith, T. Kroll, A. L. Hartig, A. Ignatov, S. Ilieva, M. Thurauf, S. Lalkovski, D. Ivanova, S. Kisyov, W. Korten, M.D. Salsac, M. Zielinska, N. Marginean, D.G. Ghita, R. Lica, C. M. Petrache, A. Astier, and R. Leguillon, Phys. Rev. C **90**, 067301 (2014).
[11] M. Albers, Nucl. Phys. A **899**, 1 (2013).
[12] S. Raman, C. W. Nestor, and P. Tikkanen, At. Data Nucl. Data Tables **78**, 1 (2001).
[13] A. Bohr and B. R. Mottelson, *Nuclear Structure II*, 1st ed. (Benjamin, New York, 1974).
[14] P. O. Hess, J. A. Maruhn, and W. Greiner, J. Phys. G:Nucl. Phys. **7**, 737 (1981).
[15] G. Gneuss and W. Greiner, Nucl. Phys. A **171**, 449 (1971).
[16] M. A. Caprio, D. J. Rowe, and T. A. Welsh, Comput. Phys. Commun. **180**, 1150 (2009).
[17] T. A. Welsh and D. J. Rowe, Comp. Phys. Commun. **200**, 220 (2016).
[18] D. J. Rowe, Nucl. Phys. A **735**, 372 (2004).

[19] D. J. Rowe and P. S. Turner, Nucl. Phys. A **753**, 94 (2005).
[20] M. A. Caprio, Phys. Rev. C **72**, 054323 (2005).
[21] D. J. Rowe and J. L. Wood, *Fundamentals of Nuclear Models: Foundational Models*, Vol. 2 (World Scientific, Singapore, 2010).
[22] P. S. Turner and D. J. Rowe, Nucl. Phys. **756**, 333 (2005).
[23] M. Bender, P.-H. Heenen, and P.-G. Reinhard, Rev. Mod. Phys. **75**, 121 (2003).
[24] P. Bonche, P.-H. Heenen, H. Flocard, and D. Vautherin, Phys. Lett. B **175**, 387 (1986).
[25] J.-F. Berger, M. Girod, and D. Gogny, Nucl. Phys. A **502**, 85 (1989).
[26] J. Meng, W. Zhang, S. G. Zhou, H. Toki, and L. S. Geng Eur. Phys. J. A **25**, 23 (2005).
[27] R. Fossion, D. Bonatsos, and G. A. Lalazissis, Phys. Rev. C **73**, 044310 (2006).
[28] P. Klüpfel, P.-G. Reinhard, T. J. Bürvenich, and J. A. Maruhn, Phys. Rev. C **79**, 034310 (2009).
[29] W. J. Huang, G. Audi, M. Wang, F. G. Kondev, S. Naimi, and X. Xu, Chin. Phys. C **41**, 030002 (2017).
[30] J. Terasaki, P.-H. Heenen, H. Flocard, and P. Bonche Nucl. Phys. A **600**, 371 (1996).
[31] J. A. Maruhn, P.-G. Reinhard, P. D. Stevenson, and A. S. Umar, Comput. Phys. Commun. **185**, 2195 (2014).
[32] P. Klüpfel, J. Erler, P.-G. Reinhard, and J. A. Maruhn, Eur. Phys. J. A **37**, 343 (2008).
[33] T. R. Rodríguez and J. L. Egido, Phys. Rev. C **81**, 064323 (2010).
[34] T. R. Rodríguez, Phys. Rev. C **90**, 034306 (2014).
[35] J. Berger, M. Girod, and D. Gogny, Nucl. Phys. A **428**, 23 (1984).
[36] T. Materna, W. Urban, K. Sieja, U. Koster, H. Faust, M. Czerwinski, T. Rzaca-Urban, C. Bernards, C. Fransen, J. Jolie, J. M. Regis, T. Thomas, and N. Warr, Phys. Rev. C **92**, 034305 (2015).
[37] M. Borrajo, T. R. Rodríguez, and J. L. Egido, Phy. Lett. B **746**, 341 (2015).
[38] J. L. Egido, M. Borrajo, and T. R. Rodríguez, Phys. Rev. Lett. **116**, 052502 (2016).
[39] T. R. Rodríguez, Eur. Phys. J. A **52**, 190 (2016).